

Translational Control of Entrainment and Synchrony of the Suprachiasmatic Circadian Clock by mTOR/4E-BP1 Signaling

Ruifeng Cao,¹ Barry Robinson,² Haiyan Xu,³ Christos Gkogkas,¹ Arkady Khoutorsky,¹ Tommy Alain,¹ Akiko Yanagiya,¹ Tatiana Nevarko,¹ Andrew C. Liu,³ Shimon Amir,^{2,*} and Nahum Sonenberg^{1,*}

¹Department of Biochemistry and Goodman Cancer Research Center, McGill University, Montreal, QC H3A 1A3, Canada

²Center for Studies in Behavioral Neurobiology, Concordia University, Montreal, QC H4B 1R6, Canada

³Department of Biological Sciences, The University of Memphis, Memphis, TN 38152, USA

*Correspondence: shimon.amir@concordia.ca (S.A.), nahum.sonenberg@mcgill.ca (N.S.)

<http://dx.doi.org/10.1016/j.neuron.2013.06.026>

SUMMARY

Protein synthesis is critical for circadian clock function, but little is known of how translational regulation controls the master pacemaker in mammals, the suprachiasmatic nucleus (SCN). Here we demonstrate that the pivotal translational repressor, the eukaryotic translational initiation factor 4E binding protein 1 (4E-BP1), is rhythmically regulated via the mechanistic target of rapamycin (mTOR) signaling in the SCN and preferentially represses vasoactive intestinal peptide (*Vip*) mRNA translation. Knockout (KO) of *Eif4ebp1* (gene encoding 4E-BP1) leads to upregulation of VIP and higher amplitude of molecular rhythms in the SCN. Consequently, the 4E-BP1 null mice exhibit accelerated re-entrainment to a shifted light/dark cycle and are more resistant to the rhythm-disruptive effects of constant light. Conversely, in *Mtor*^{+/-} mice VIP expression is decreased and susceptibility to the effects of constant light is increased. These results reveal a key role for mTOR/4E-BP1-mediated translational control in regulating entrainment and synchrony of the master clock.

INTRODUCTION

Circadian rhythmicity is a fundamental biological property that orchestrates various behavioral, physiological, and metabolic processes in a wide range of organisms (Rosbash, 2009). In mammals, the master circadian clock is located in the suprachiasmatic nucleus (SCN) of the hypothalamus (Reppert and Weaver, 2002). The cellular clockwork is driven by interconnected transcriptional and posttranscriptional feedback loops (Rosbash et al., 2007; Takahashi et al., 2008). In a major negative feedback loop, the transcription factors CLOCK and BMAL1 form heterodimers and activate transcription of *Period* (*Per*) and *Cryptochrome* (*Cry*) genes. In turn, PER and CRY proteins associate with CLOCK/BMAL1 heterodimers and repress their own gene transcription.

SCN neurons are heterogeneous in their oscillatory activities, neuropeptide expression, and responses to light (Welsh et al., 1995; Herzog et al., 1998; Antle and Silver, 2005). Cellular oscillators in the SCN are coupled to form a coherent and stable oscillator network (Aton and Herzog, 2005; Welsh et al., 2010). Intercellular synchronization confers robustness and accuracy to SCN-generated rhythms and distinguishes SCN from peripheral oscillators, where coupling is weak (Yamazaki et al., 2000; Yamaguchi et al., 2003; Liu et al., 2007a). Although the mechanisms of such synchrony are not fully understood, recent evidence points to an essential role for vasoactive intestinal peptide (VIP) (Shen et al., 2000; Harmar et al., 2002; Colwell et al., 2003; Aton et al., 2005; Maywood et al., 2006). VIP is a 28 amino acid neuropeptide, which is cleaved from the precursor protein prepro-VIP encoded by the *Vip* gene (Gozes and Brenneman, 1989). In the SCN, *Vip* is expressed by a subset of ventromedial SCN neurons (Abrahamson and Moore, 2001). However, the molecular mechanisms regulating prepro-VIP synthesis are not understood.

Protein synthesis is controlled primarily at the step of mRNA translation initiation (Sonenberg and Hinnebusch, 2009). A critical event in this process is the association of the eukaryotic translation initiation factor 4E (eIF4E) with the mRNA 5' m⁷GpppN (where N is any nucleotide) cap structure. eIF4E binding to the cap structure is controlled by the eIF4E-binding proteins (4E-BPs). Binding of 4E-BPs to eIF4E causes inhibition of cap-dependent translation initiation and is relieved by 4E-BP phosphorylation through the mechanistic target of rapamycin (mTOR) signaling (Gingras et al., 1999). mTOR is an evolutionarily conserved Ser/Thr kinase that forms two different multi-protein complexes, mTOR complex 1 (TORC1) and mTORC2, which couple extracellular and intracellular signals (growth factors, energy status, nutrient availability, and stress) with cellular metabolic resources to balance anabolic and catabolic processes (Laplante and Sabatini, 2012). In the developing brain, mTOR controls neuronal survival and differentiation, neurite growth, and synaptogenesis (Cao et al., 2009). In the adult brain, mTOR mediates various forms of synaptic plasticity and plays an important role in learning and memory (Costa-Mattioli et al., 2009). In the hypothalamus, mTOR functions as a homeostatic sensor to control food intake and body weight (Cota et al., 2006).

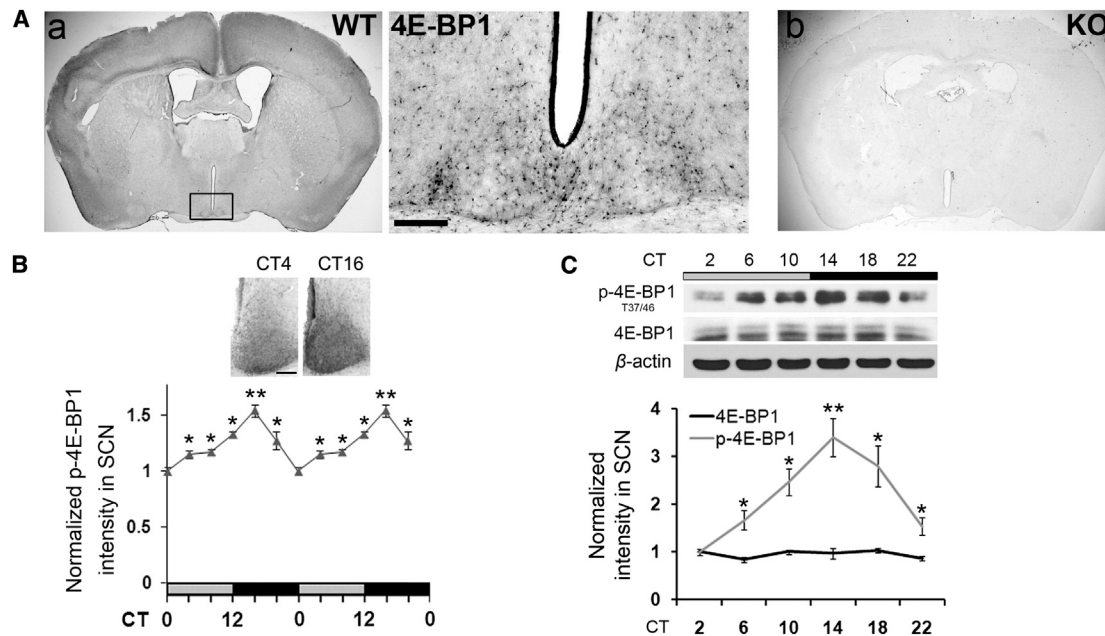


Figure 1. Expression and Circadian Phosphorylation of 4E-BP1 in SCN

(A) Bright-field microscopy images showing 4E-BP1 expression in the brain of WT (a) and *Eif4ebp1* KO (b) mice. In subpanel (a), the framed area is magnified to the right. Scale bar: 100 μ m.

(B) Circadian 4E-BP1 phosphorylation (at Thr37/Thr46) in the SCN. Double-plotted line graph shows a curve of normalized p-4E-BP1 staining intensity in the SCN. The values are presented as the mean \pm SEM. Representative microscopic images at CT4 and CT16 are shown above. * $p < 0.05$ versus CT0, ** $p < 0.01$ versus CT0. Scale bar: 100 μ m.

(C) Circadian phosphorylation of 4E-BP1 (at Thr37/Thr46) in the SCN. 8% polyacrylamide gel was used. Note that phosphorylation of 4E-BP1 exhibited different levels with circadian time, while 4E-BP1 level did not change. β -actin was used as a protein loading control. Quantitative data are from three biological replicates. The values are presented as the mean \pm SEM. * $p < 0.05$ versus CT2, ** $p < 0.01$ versus CT2. In each experiment, SCN tissue from five mice was pooled for each time point. Half of the lysate was used for detecting phosphorylation of 4E-BP1 and the other half was used for 4E-BP1 and β -actin blotting. See also Figure S1.

Recent work has begun to reveal key roles for mTOR signaling in circadian clocks. Notably, mTOR activity exhibits robust circadian rhythms in the SCN (Cao et al., 2011), and light exposure activates mTOR signaling in a phase-dependent manner (Cao et al., 2008). Pharmacological inhibition of mTOR activation decreases light-induced PER protein expression and modulates behavioral phase shifts in animals (Cao et al., 2010). In *Drosophila*, elevation of mTOR activity by genetic manipulation lengthens the circadian period (Zheng and Sehgal, 2010). One of the best-studied roles of mTORC1 is control of protein synthesis via phosphorylation of its major targets, 4E-BPs and S6 kinases (Topisirovic and Sonenberg, 2011). Interestingly, 4E-BPs are strongly phosphorylated in the SCN, in striking contrast with other brain regions (Cao and Obrietan, 2010). Furthermore, 4E-BP phosphorylation in the SCN is stimulated by light in an mTOR-dependent manner, suggesting the involvement of 4E-BPs in the SCN clock physiology (Cao et al., 2008). Here, using a combination of behavioral, biochemical, and molecular approaches, we investigated the functions of 4E-BP1 in the mammalian circadian clock. We show that 4E-BP1 regulates entrainment and synchrony of the SCN clock by repressing *Vip* mRNA translation, thus demonstrating a key role for mTOR/4E-BP1-mediated translational control in the master pacemaker.

RESULTS

Circadian Regulation of 4E-BP1 Phosphorylation in SCN

Abundant expression of 4E-BP1 was detected in the SCN, as compared to other hypothalamic brain regions (Figure 1A left). High-magnification imaging revealed that 4E-BP1 was extensively expressed in the SCN (Figure 1A middle). To confirm the specificity of the 4E-BP1 immunostaining, we performed parallel staining on brain sections from *Eif4ebp1* (gene encoding 4E-BP1) knockout (KO) mice (see below). No signal was detected in the KO brain (Figure 1A right).

Next, we examined 4E-BP1 phosphorylation in the SCN over a 24 hr period when mice were kept under constant dark (DD). mTOR-dependent phosphorylation of 4E-BP1 at Thr37 and Thr46 primes 4E-BP1 for subsequent phosphorylation at Ser65 and Thr70 and is therefore an indicator of 4E-BP1 activity (Gingras et al., 1999). Strong 4E-BP1 phosphorylation (at Thr37/Thr46) was detected in the SCN by immunostaining, with highest level at circadian time (CT) 16 and lowest level at CT0 (CT4, CT8, CT12, and CT20 versus CT0, $p < 0.05$; CT16 versus CT0, $p < 0.01$, analysis of variance [ANOVA], Figure 1B). Importantly, 4E-BP1 phosphorylation is mTOR dependent, as rapamycin decreased the signal (Figure S1A). In contrast to SCN, other brain regions exhibited weak 4E-BP1 phosphorylation

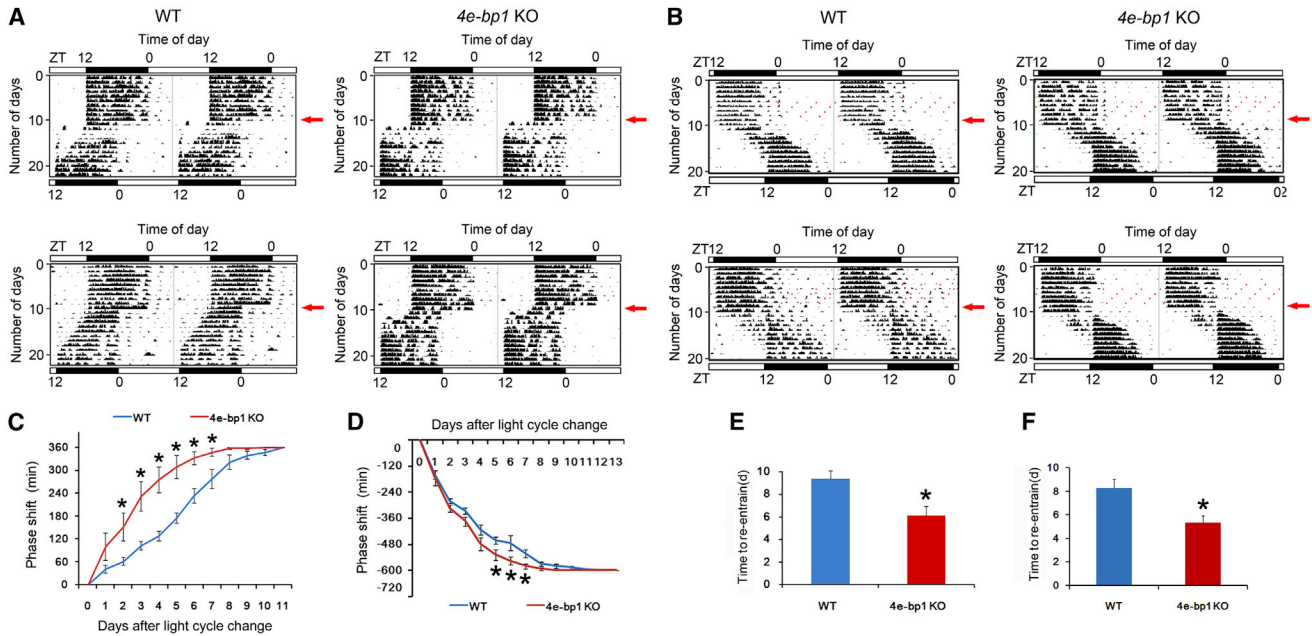


Figure 2. Accelerated Circadian Behavioral Re-entrainment in *Eif4ebp1* KO Mice

(A and B) Representative double-plotted actograms of wheel-running activities from two WT (left) and two *Eif4ebp1* KO mice (right). The x axis (top) indicates the Zeitgeber time (ZT) of the day. The y axis (left) indicates the number of days during the experiment. For these experiments, the animals were entrained to a 12 hr/12 hr light/dark (LD) cycle for 10 days, and on the 11th day, the LD cycle was either advanced for 6 hr (light on at previous ZT18) (A) or delayed for 10 hr (light off at previous ZT22) (B). Red arrows (right) indicate the day when the light cycle was shifted. (C and D) Line graphs showing the daily phase advance (C) or delay (D) of wheel-running activities following a 6 hr advancing LD cycle shift (C) or a 10 hr delaying LD cycle shift (D). Values are presented as the mean \pm SEM. Each data point is averaged from nine mice. * $p < 0.05$ KO versus WT by ANOVA. (E and F) Histograms showing time (in days) needed for the mice to re-entrain to a 6 hr LD cycle advance (E) or a 10 hr LD cycle delay (F). Values are presented as the mean \pm SEM. Each data point is averaged from nine mice. * $p < 0.05$ KO versus WT by Student's t test. See also Figure S2.

(Figure S1A), consistent with low 4E-BP1 expression in these regions. Consistent with the immunostaining results, western blotting revealed that 4E-BP1 phosphorylation was highest at around CT14 and lowest at around CT2 (CT6, CT10, CT18, and CT22 versus CT2, $p < 0.05$; CT14 versus CT2, $p < 0.01$, ANOVA, Figure 1C and Figure S1B). Total 4E-BP1 and *Eif4ebp1* mRNA level did not oscillate in the SCN (Figure S1C). ERK/MAPK contributes to circadian mTOR activity in the SCN (Cao et al., 2011). As expected, MEK inhibitor U0126 decreased 4E-BP1 phosphorylation in the SCN (Figure S1D). Together, these findings indicate that 4E-BP1 activity is controlled by the circadian clock via mTOR signaling in the SCN.

Accelerated Re-entrainment of Circadian Behavior in *Eif4ebp1* KO Mice

To investigate the potential roles of 4E-BP1 in the circadian clock, we utilized an *Eif4ebp1* KO mouse strain (Tsukiyama-Kohara et al., 2001). Confocal microscopic examination of DRAQ5 (a nuclear stain)-labeled sections revealed no difference in the histological features of SCN tissues between wild-type (WT) and KO mice (Figure S2A). To study the effects of *Eif4ebp1* gene deletion on circadian behavior, mice were kept in a 12 hr/12 hr light/dark (LD) cycle for 10 days and then released into DD for 9 days. The KO mice entrained normally to the LD cycle and displayed robust free-running rhythms of locomotor activities in DD (Figure S2B). However, the circadian period

(tau) of KO mice was slightly decreased compared to the WT mice (KO versus WT, 23.67 ± 0.06 , $n = 12$ versus 23.81 ± 0.03 , $n = 12$, $p < 0.05$, Student's t test; Figure S2C). Dark pulses applied during the light phase did not induce significant wheel-running activities in the mice, and no difference was noted between WT and KO mice (Figure S2D).

Next, to further characterize the circadian behavior of the *Eif4ebp1* KO mouse, we used a "jet lag" model to study clock entrainment. For this purpose, mice were kept in a 12 hr/12 hr LD cycle for 10 days, followed by an abrupt 6 hr phase advance of the LD cycle, with light on at zeitgeber time (ZT) 18. During re-entrainment, the mice displayed increased nighttime rest and daytime running and gradually re-entrained to the new LD cycle (Figure 2A). Notably, the KO mice re-entrained more quickly than the WT mice (Figure 2A). From day 2 to day 7 following the LD cycle shift, the KO mice exhibited a larger phase advance than the WT mice (KO versus WT, $p < 0.05$, ANOVA, Figure 2C), and the time to re-entrain was ~40% shorter for the KO mice (KO versus WT, $p < 0.05$, Student's t test; Figure 2E). In the second experiment, after the mice were entrained to a 12 hr/12 hr LD cycle for 10 days, the LD cycle was abruptly delayed by 10 hr (light off at ZT22). Similar to the phase advancing experiment, during re-entrainment, both the WT and the KO mice displayed increased daytime running and nighttime rest (Figure 2B). However, the KO mice re-entrained more quickly to the delayed LD cycle (Figure 2B). From day 5

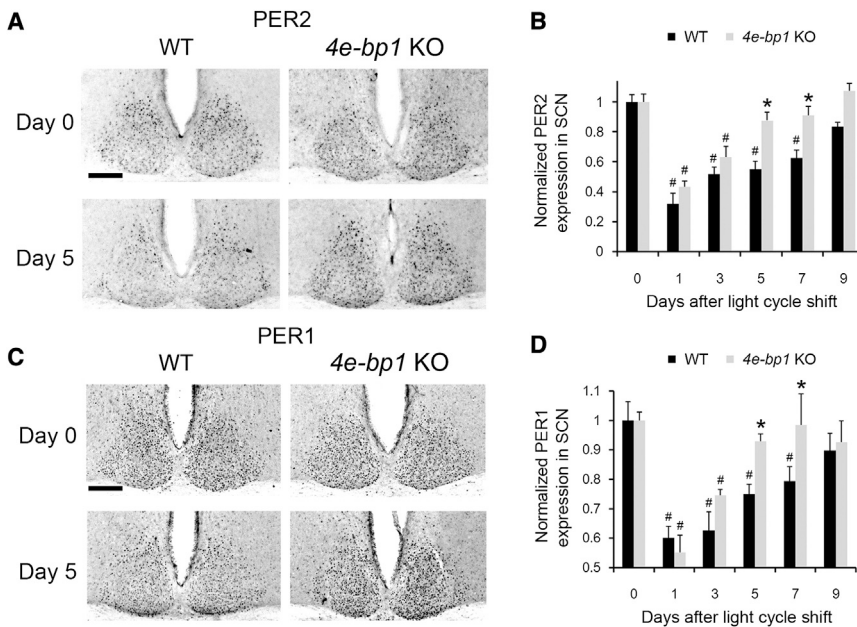


Figure 3. Accelerated PERIOD Rhythm Resynchronization in *Eif4ebp1* KO Mice

(A–D) Representative microscopic images of PER2 (A) and PER1 (C) immunostaining in the SCN. WT and *Eif4ebp1* KO animals were entrained in a 12 hr/12 hr LD cycle for 10 days, and on the 11th day, the LD cycle was advanced for 6 hr (light on at previous ZT18). Mice were sacrificed at ZT12 before and different days after the LD cycle shift. Representative images are shown before (Day 0) and 5 days after the LD cycle shift (Day 5). Scale bars: 100 μ m. The quantitative data for all time points are shown in (B) for PER2 and (D) for PER1. PER levels at ZT12 on Day 0 are normalized to be “1” in WT and KO SCN. Values are presented as the mean \pm SEM. Each data point is averaged from eight mice. # p < 0.05 versus Day 0; * p < 0.05 versus WT by ANOVA. See also Figure S3.

to day 7 following the shift, the KO mice exhibited a larger phase delay than the WT mice (KO versus WT, p < 0.05, ANOVA, Figure 2D), and the time to re-entrain was \sim 40% shorter for the KO mice (KO versus WT, p < 0.05, Student’s t test; Figure 2F).

Because dark pulses did not induce significant wheel-running activities in the KO mice (see Figure S2D), the accelerated re-entrainment is unlikely due to enhanced negative masking. ERK phosphorylation and Jun expression are sensitive and reliable markers of photic stimulation of the SCN clock (Kornhauser et al., 1992; Obrietan et al., 1998). Light-induced ERK phosphorylation (at Thr202/Tyr204) and c-Jun expression in the SCN were not different in the KO mice (Figures S3A and S3B; KO versus WT, p > 0.05, ANOVA). Further, as a core component of the clock feedback loop, light-pulse-induced PER1 was not altered in the core region of SCN of the KO mice (Figures S3C and S3D). Basal PER levels were not changed in the brain of the KO mice (Figure S3E), indicating that 4E-BP1 does not regulate cellular PER expression. Taken together, these results demonstrate that although masking behavior and photic entrainment pathway are intact, re-entrainment of circadian behavior is accelerated in *Eif4ebp1* KO mice.

Accelerated Resynchronization of PER Rhythms in *Eif4ebp1* KO Mice

When animals are stably entrained to the 12 hr/12 hr LD cycle, PER (including PER1 and PER2) rhythms in different regions of the SCN are synchronized and the overall PER levels in the SCN peak at around the light/dark transition (ZT12) (Hastings et al., 1999; Field et al., 2000). When the LD cycle is abruptly shifted, PER rhythms within different regions of the SCN become desynchronized due to their different re-entraining speeds (Reddy et al., 2002; Nagano et al., 2003; Albus et al., 2005; Nakamura et al., 2005; Davidson et al., 2009). Consequently, PER levels of the entire SCN are lower at ZT12 than when the

clock is well entrained. As SCN cells become resynchronized, the PER levels at ZT12 recover to the original levels prior

to the LD cycle shift (Amir et al., 2004). Thus, to investigate the molecular mechanisms responsible for the accelerated re-entrainment of circadian behavior in the *Eif4ebp1* KO mice, we measured PER levels in the SCN at ZT12 before and after the LD cycle shift.

Before the LD cycle shift, PER1 and PER2 levels in the KO mice were not different from those in the WT animals (day 0, Figures 3A and 3C). In contrast, on day 5 after the 6 hr advancing LD cycle shift, PER1 and PER2 levels were higher in the SCN of the KO mice, suggesting better resynchronization of cellular clocks by day 5 (Figures 3A and 3C). Quantitations of PER levels before and after the light cycle shift are presented in Figures 3B and 3D. One day after the LD cycle shift, PER levels at ZT12 were dramatically decreased in the WT mice. They increased with time and reached preshifted control (day 0) levels 9 days after the light cycle shift (days 1, 3, 5, and 7 versus day 0, p < 0.05; day 9 versus day 0, p > 0.05, ANOVA, Figures 3B and 3D). In the KO mice, PER1/2 at ZT12 decreased to levels similar to those in WT mice following the light cycle shift, indicating a similar degree of desynchronization. Significantly, however, in the SCN of KO mice PER1/2 reached the preshifted levels 5 days after the light cycle shift, \sim 40% faster than in the WT mice (days 1 and 3 versus day 0, p < 0.05; days 5, 7, and 9 versus day 0, p > 0.05, ANOVA). Thus, on days 5 and 7 following the light cycle shift, PER levels in the SCN of the KO mice were significantly higher than in the WT mice (days 5 and 7, KO versus WT, p < 0.05, ANOVA, Figures 3B and 3D).

Notably, the PER staining data are remarkably consistent with the behavioral entrainment data (see Figure 2), showing that the WT mice re-entrained to a shifted light cycle in approximately 9 days, whereas the KO mice reach a new steady phase in approximately 5 days. Taken together, these results support the idea that KO mice re-entrain more quickly because cellular clocks in the SCN of these mice resynchronize faster to the shifted LD cycle.

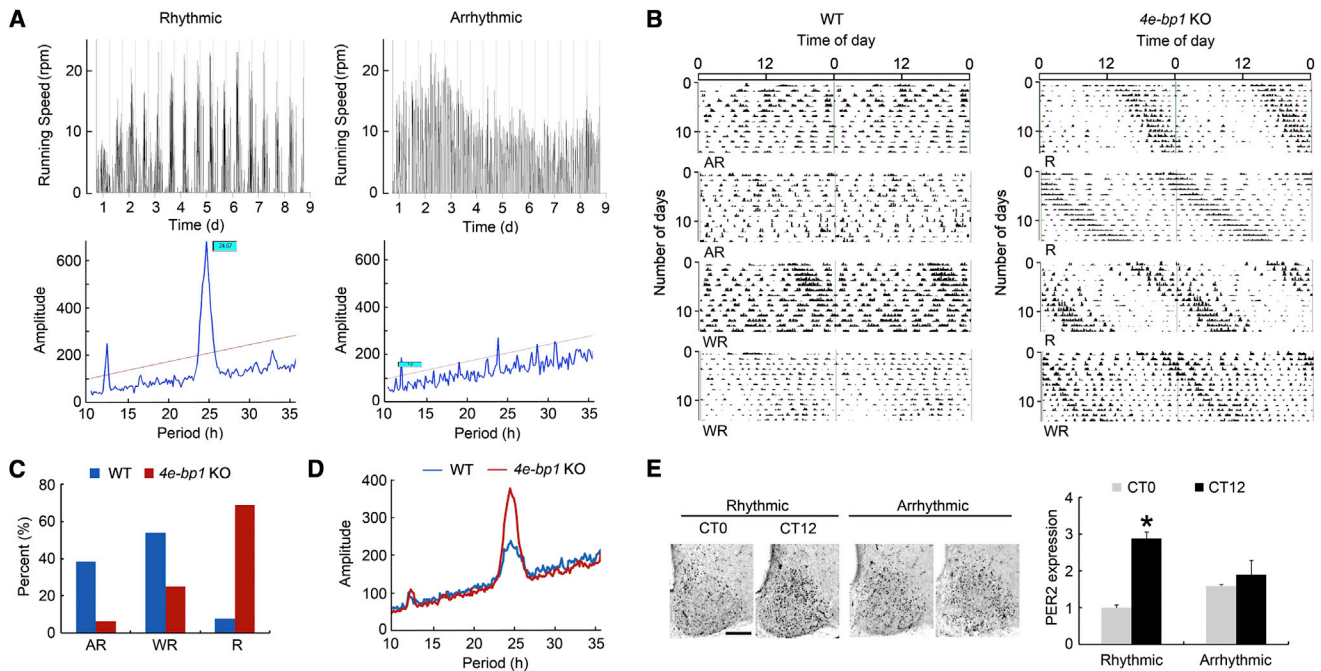


Figure 4. Resistance to Constant Light-Induced Clock Desynchrony in *Eif4ebp1* KO Mice

(A) Constant light (LL)-induced arrhythmic wheel-running behavior in mice. Representative wheel-running speed line graphs (top) and periodograms (bottom) from a rhythmic (left) and an arrhythmic (right) mouse in LL. Note that in the periodogram of the rhythmic animal, a main peak is seen at around 25 hr, indicating lengthened circadian period under LL. In the arrhythmic periodogram, there is no main peak.

(B and C) Representative wheel-running actograms of mice in LL (B). Actograms from four WT (left) and four KO (right) mice are shown. R, rhythmic; AR, arrhythmic; WR, weakly rhythmic. The percentages of three types of behavior are shown in (C).

(D) Pooled periodograms from all mice used in the experiment. Note that the overall rhythmicity of KO mice was stronger compared to the WT mice, as indicated by a higher amplitude of the main peak of the periodogram. Thirteen WT and 16 KO mice were used in the experiment.

(E) PER2 expression in the SCN. Left: Representative microscopic images of PER2 staining in the SCN. Right: Quantitation of PER2 levels in the SCN. The values are presented as the mean \pm SEM. * $p < 0.05$ versus CT0. Note that in the arrhythmic mice, PER2 levels were not different at the two time points separated by 12 hr. For this experiment, both WT and KO mice were used. PER2 levels were not different between WT and KO mice. Scale bar: 100 μ m.

Resistance to Constant Light-Induced Clock Desynchrony in *Eif4ebp1* KO Mice

Prolonged exposure to constant light (LL) extends endogenous circadian period and induces arrhythmic behavior in a sizable percentage of animals, depending on the light intensity and animal species (Daan and Pittendrigh, 1976). In the arrhythmic animals, LL disrupts the coupling among individual SCN neurons without affecting intracellular clock function (Ohta et al., 2005). To study the effect of LL on circadian behavior and PER2 expression in the SCN, *Eif4ebp1* KO and WT mice were first housed in regular colony cages in LL (200 lx at cage level) for 14 days. Subsequently, the animals were transferred to individual cages equipped with running wheels in LL (55 lx at cage level) and their circadian behavior was recorded for 14 days. The wheel-running behavior in LL was classified into three types based on the amplitude of the main peak of the periodograms: (1) rhythmic (R, amplitude > 200 , Figure 4A left); (2) arrhythmic (AR, amplitude ≤ 50 or no main peak, Figure 4A right) and (3) weakly rhythmic (WR, $50 < \text{amplitude} \leq 200$).

LL induced all three types of behavior in both WT and *Eif4ebp1* KO animals. Most WT mice were either arrhythmic (AR) or weakly rhythmic (WR), while most KO mice were rhythmic (R) in LL (Figure 4B). Distribution of the three types of behavior (AR, WR,

and R) in both genotypes is quantified in Figure 4C. Strikingly, a smaller percentage of KO mice (6.3%, 1/16) exhibited arrhythmic behavior than did WT mice (38.5%, 5/13) (KO versus WT, $p < 0.05$, χ^2 test). The pooled periodograms from all the mice used in the experiment are shown in Figure 4D. The main peak of the periodogram is higher in the KO mice than in the WT mice, demonstrating stronger rhythmicity in the KO mice in LL. To verify that the rhythms of clock protein expression are disrupted in behaviorally arrhythmic mice, PER2 was immunostained in the SCN at CT0 and CT12 for the rhythmic mice and at two random time points 12 hr apart for the arrhythmic mice. CT12 was defined as the onset time of the active phase, and CT0 was defined as the time point 12 hr apart from CT12. As expected, PER2 was not rhythmic in the SCN of behaviorally arrhythmic mice (KO or WT), as compared to the rhythmic mice (Figure 4E). Thus, these data show that *Eif4ebp1* KO mice are more resistant to LL-induced disruption of circadian behavioral and PER2 rhythms, consistent with enhanced synchrony in the SCN cells.

Regulation of *Vip* mRNA Translation by mTOR/4E-BP1 Signaling

VIP plays a critical role in mediating synchrony in SCN cells. To investigate the mechanisms of enhanced re-entrainment and

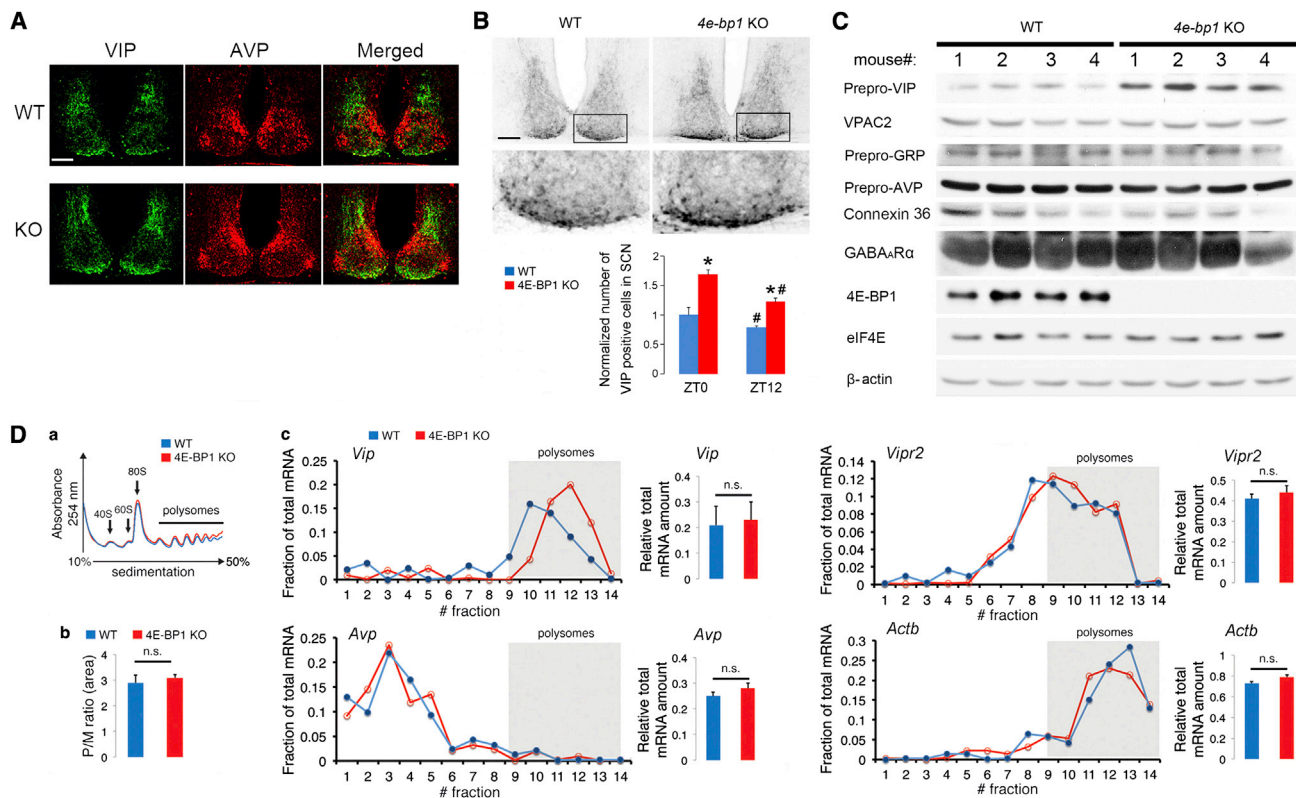


Figure 5. Regulation of VIP Expression by 4E-BP1

(A) Confocal microscopic images showing expression of VIP (green) and AVP (red) in the SCN. For these experiments, the mice were entrained and sacrificed at ZT0. Note that VIP and AVP expression pattern in the *Eif4ebp1* KO SCN was similar to that in the WT SCN. Scale bar: 100 μ m.

(B) Top: Representative bright-field microscopy images showing VIP immunostaining in the SCN. For these experiments, mice were sacrificed at ZT0. Note that number of VIP-positive cells was increased in the *Eif4ebp1* KO SCN. Scale bars: 100 μ m. Framed regions are magnified to below. Bottom: Quantitation of number of VIP-positive cells in the SCN. The values are presented as the mean \pm SEM. * $p < 0.05$ versus WT; # $p < 0.05$ versus ZT0 by ANOVA. Four animals were used for each group.

(C) Western blots of whole-forebrain lysates. For these experiments, animals were sacrificed at ZT0. The numbers 1–4 indicate four different animals for each group. Note that prepro-VIP but not VPAC2, prepro-GRP, prepro-AVP, Connexin 36, or GABA_AR α was significantly increased in the brain of *Eif4ebp1* KO mice. eIF4E and β -actin were used as loading controls. See Results for quantitation of the blots.

(D) Brain polysome profiling assay. (a) Polysome profiles from whole-brain lysates. The positions of the 40S, 60S, and 80S ribosome peaks and polysomes are indicated. (b) Polysome to monosome ratio. No difference was found between WT and *Eif4ebp1* KO profiles ($n = 3$, $p > 0.05$, Student's *t* test). (c) Left figures show qRT-PCR results of *Vip*, *Avp*, *Vipr2*, and *Actinb* on RNA extracted from whole-brain polysome fractions. qRT-PCR results on total mRNA extracted from brain lysates are shown to the right. Note that for *Vip* mRNA distribution, a shift to the right (heavier gradient fractions) indicates increased translation initiation ($n = 3$). No significant shifts were detected on distribution profiles of *Avp*, *Vipr2*, or *Actinb* mRNAs. No differences were found in *Vip*, *Avp*, *Vipr2*, and *Actinb* transcription between WT and *Eif4ebp1* KO ($n = 3$, $p > 0.05$ by Student's *t* test). See also Figure S4.

synchrony of the SCN clock in *Eif4ebp1* KO mice, we first studied VIP expression in these animals. Using double immunofluorescent labeling, we first examined the expression pattern of VIP and arginine vasopressin (AVP) in the SCN. AVP is generally used as a neuropeptide marker for the dorsolateral SCN (Abrahamson and Moore, 2001). Confocal microscopic imaging revealed that VIP was expressed in a subset of ventromedial (core) SCN neurons, while AVP was expressed in some cells in the dorsal and lateral (shell) SCN (Figure 5A). The spatial distribution of VIP and AVP was similar in the SCN of KO and WT animals. Immunohistochemical staining also revealed robust VIP expression in the SCN (Figure 5B and Figure S4A). In both the WT and the KO mice, expression of VIP at ZT12 was decreased compared to ZT0 (ZT12 versus ZT0, $p < 0.05$, ANOVA), which is

consistent with a previous report (Takahashi et al., 1989). Interestingly, VIP level was increased by ~ 1 -fold in the *Eif4ebp1* KO mice at both ZT0 and ZT12 (KO versus WT, $p < 0.05$, ANOVA) (Figure 5B), suggesting constitutive repression of VIP expression by 4E-BP1.

To investigate the mechanisms underlying VIP increase in *Eif4ebp1* KO mice, we examined the expression of the VIP precursor protein, prepro-VIP, in the brain. We used whole-brain lysate for western blotting analysis, because the available antibody was not sensitive enough to detect prepro-VIP in the small amount of SCN lysate and because VIP is extensively expressed in all brain regions (Gozes and Brenneman, 1989). Prepro-VIP level was increased significantly in the brain of *Eif4ebp1* KO mice (normalized band intensities: KO versus WT, 3.88 ± 0.36

versus 1 ± 0.18 , $p < 0.05$, Student's t test; Figure 5C). In contrast, expression of VPAC2 (the VIP receptor expressed in the SCN), and of the precursor proteins of other neuropeptides implicated in the SCN synchrony (Piggins et al., 1995; Maywood et al., 2011), including prepro-GRP and prepro-AVP, was not changed (Figure 5C). In addition to the neuropeptides, we examined other proteins involved in SCN synchrony, including GABA_A receptor (Liu and Reppert, 2000; Colwell et al., 2003; Albus et al., 2005) and gap junction protein Connexin 36 (Long et al., 2005). The levels of Connexin 36 and the GABA_A receptor α subunit were not altered in the *Eif4ebp1* KO brain (Figure 5C). Furthermore, the expression of the 4E-BP1 binding partner, eIF4E, was not changed (Figure 5C). These results demonstrate specific regulation of prepro-VIP by 4E-BP1.

To complement the *in vivo* data, we studied prepro-VIP expression in mouse Neuro2A and human SHEP neuroblastoma cells (Waschek et al., 1988). Treatment of Neuro2A cells with the specific mTOR active-site inhibitor, PP242, resulted in reduced prepro-VIP levels and in dephosphorylation of 4E-BP1 after 3 hr (Figure S4B). To determine whether the effect of mTOR inhibition on prepro-VIP expression is dependent on 4E-BP1, we knocked down 4E-BP1 in SHEP cells using lentivirus (Figure S4C). Prepro-VIP was increased by ~ 1 -fold in 4E-BP1 knockdown cells. Rapamycin decreased 4E-BP1 phosphorylation and inhibited prepro-VIP expression in control cells (scrambled), but not in 4E-BP1 knockdown cells (sh4e-bp1) (Figure S4C). Serum stimulation induced strong prepro-VIP expression in control cells, but to a lesser extent in 4E-BP1 knockdown cells (Figure S4D), indicating that inducible prepro-VIP expression is at least partially dependent on 4E-BP1. Consistent with these data, overexpression of 4E-BP1 led to a reduction in prepro-VIP (Figure S4E). Overexpression of WT eIF4E, but not the W56A mutant, which cannot bind to the mRNA cap (Gingras et al., 1999), increased prepro-VIP (Figure S4F), demonstrating that prepro-VIP synthesis is dependent on eIF4E and cap-dependent translation in neuroblastoma cells. Expression of *Vip* 5' UTR-RLuc mRNA, but not RLuc or *Grp* 5' UTR-RLuc mRNA, was enhanced in *Eif4ebp1* KO (~ 2 -fold) as compared to WT mouse embryonic fibroblasts (Figure S4G; $p < 0.05$, ANOVA). *Grp* mRNA 5' UTR has a similar length but lesser secondary structure than *Vip* mRNA 5' UTR. Thus, these results demonstrate that *Vip* mRNA translation is preferentially enhanced in 4E-BP1 KO cells.

Because 4E-BP1 inhibits translation initiation, it was anticipated that prepro-VIP upregulation in the *Eif4ebp1* KO brain is at the mRNA translation initiation step. To demonstrate this, we studied *Vip* mRNA translation by polysome profiling. Brain tissue lysate from ZT0 was fractionated by sucrose density gradient centrifugation. mRNAs for which the translation initiation rate is fast are associated with multiple ribosomes and sediment at the heavy-density fractions (Figure 5D-a). The polysome/monosome ratio was not changed in the KO brain (Figure 5D-b), indicating that the translation of most mRNAs is not changed. Next, the abundance of *Vip*, *Avp*, *Vipr2* (the gene encoding VPAC2), and *Actb* mRNAs in each fraction was quantified by qRT-PCR, and the distribution of the mRNAs was compared between the WT and KO mice (Figure 5D-c). In the KO brain, *Vip* mRNA was shifted toward the heavy-density fractions, but total *Vip* mRNA level

was not changed (Figure 5D-c), demonstrating enhanced *Vip* mRNA translation initiation. This effect on *Vip* mRNA translation was highly specific, as *Avp*, *Vipr2*, and *Actb* mRNA distribution was not changed (Figure 5D-c). Taken together, these data demonstrate that 4E-BP1 inhibits VIP expression by specifically repressing *Vip* mRNA translation initiation.

Reversal of Circadian Phenotypes in *Eif4ebp1* KO Mice by Antagonizing VIP Signaling

To study the dynamics of molecular rhythms in 4E-BP1 null mice, we made the *Eif4ebp1*^{-/-}:mPER2::LUC mice. We first examined the PER2::LUC bioluminescence expression patterns of tissue explants of the SCN and, as a representative of peripheral oscillators, the lung. No significant difference in period length and amplitude was observed between WT and KO lung explants (KO versus WT, $p > 0.05$, Student's t test; Figures 6A, 6C, and 6D), demonstrating that the circadian properties of peripheral oscillators are not changed in the KO mice. However, for the SCN rhythms, the KO explants displayed shorter period than the WT explants (WT, 25.57 hr \pm 0.39 hr, $n = 9$; KO, 24.76 hr \pm 0.14 hr, $n = 8$, KO versus WT, $p < 0.05$, Student's t test; Figures 6B and 6C), consistent with animal behavioral data (see Figure S2C). Strikingly, the amplitude of SCN rhythms was higher in the KO explants (WT, 1 \pm 0.21, $n = 9$; KO, 2.74 \pm 0.60, $n = 8$, KO versus WT, $p < 0.05$, Student's t test; Figures 6B and 6D).

The SCN pacemaker distinguishes from the peripheral oscillators in its neuronal network coupling capacity and the resulting system robustness (Liu et al., 2007a; Welsh et al., 2010). Experimental evidence and *in silico* modeling indicate that coupling strength (e.g., through VIP signaling) and phase relation between neurons can affect the amplitude of a multicellular oscillator (To et al., 2007; vanderLeest et al., 2009; Abraham et al., 2010). Thus, our results are consistent with this notion and indicate that, whereas cellular oscillators that lack functional intercellular coupling (e.g., in the lung) function normally in the 4E-BP1 null mice, changes in intercellular coupling within the SCN network (e.g., elevated VIP signaling) can influence the properties of the SCN clock. To investigate whether VIP signaling is responsible for the increased amplitude in the KO mice, we applied VPAC2 antagonist PG99-465 (Cutler et al., 2003) to the SCN explants from KO mice. Low concentration (50 nM) of PG99-465 reversibly decreased the amplitudes of KO explants to a level that is similar to WT explants (Figures 6E and 6F). These results indicate that the amplitude increase in KO explants is caused by VIP-dependent enhancement of coupling in SCN cells.

Next, to test whether the VPAC2 antagonist can reverse the faster entrainment behavioral phenotype in 4E-BP1 null mice, *Eif4ebp1* KO mice were infused with PG99-465 (100 μ M, 4 μ l) or vehicle (physiological saline, 4 μ l) into the lateral ventricle at ZT15, before the light cycle was advanced for 6 hr (light on at ZT18). Both groups of mice re-entrained to the new LD cycle. Notably, however, the mice infused with PG99-465 re-entrained more slowly than those infused with saline (Figure 6G). From day 2 to day 4 following the LD cycle shift, PG99-465-infused mice exhibited a smaller phase advance than control (PG99-465 versus vehicle, $p < 0.05$, ANOVA, Figure 6H). Together, these results demonstrate that VIP overexpression in the SCN underlies the phenotypes of *Eif4ebp1* KO mice.

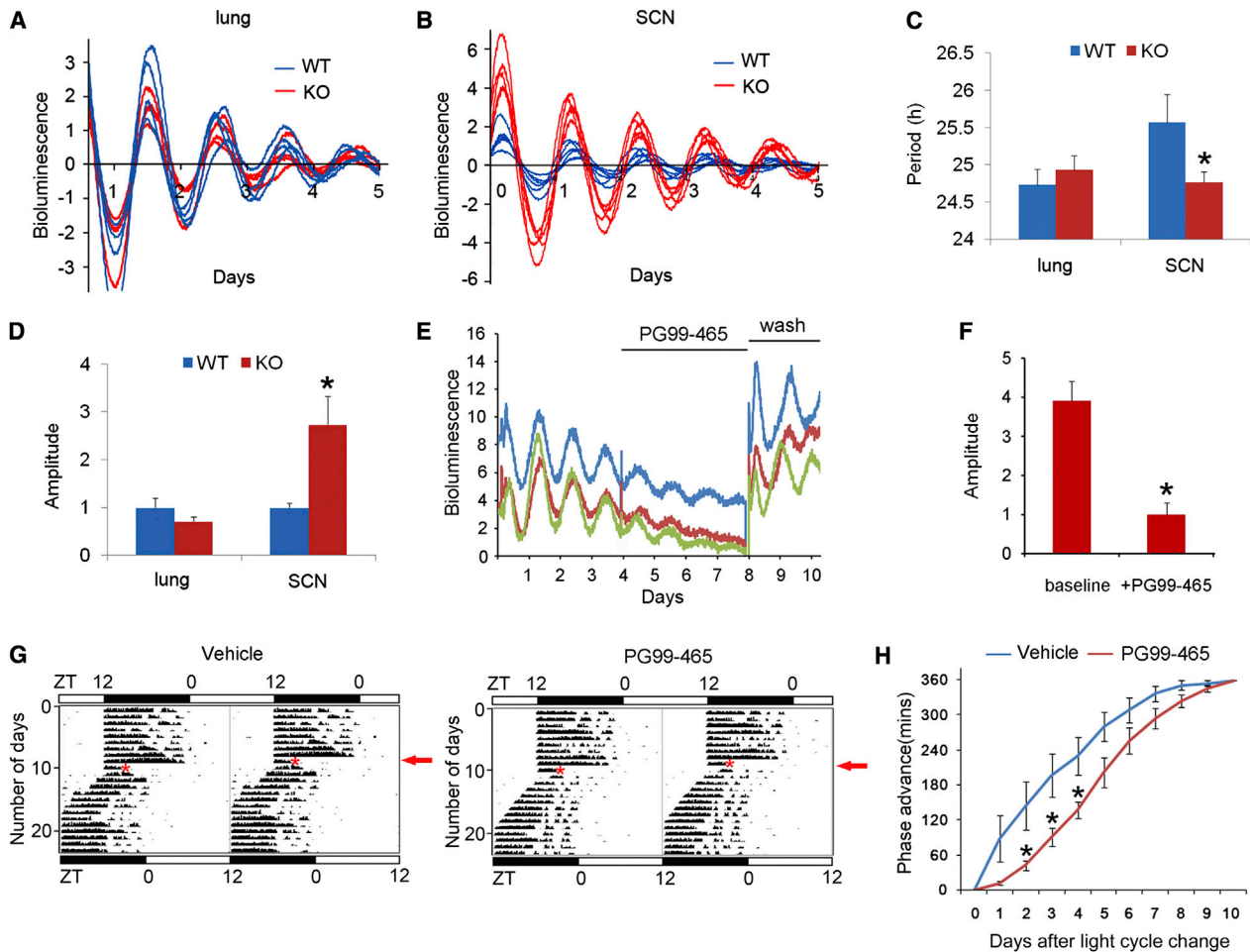


Figure 6. Reversal of Phenotypes in *Eif4ebp1* KO Mice by Antagonizing VIP Signaling

(A and B) mPER2::LUC bioluminescence patterns of lung (A) and SCN (B) explants: representative plots of lung showing similar amplitudes and periods between WT and KO mice, but representative plots of SCN showing higher amplitudes and shorter periods in the KO animals. Each plot was from one SCN explant. (C and D) Histograms showing period (C) and relative amplitude (D) of mPER2::LUC bioluminescence rhythms from lung and SCN explants. The values are presented as the mean \pm SEM. Eight to twelve animals were used for each group. * $p < 0.05$ versus WT.

(E) mPER2::LUC bioluminescence patterns of SCN explants from *Eif4ebp1* KO mice. Each plot was from one explant. Note that VPAC2 antagonist PG99-465 (50 nM) decreased amplitudes of mPer2::Luc rhythms in a reversible manner.

(F) Histograms showing relative amplitudes of mPER2::LUC bioluminescence rhythms of SCN explants from *Eif4ebp1* KO mice before and after PG99-465 treatment. The values are presented as the mean \pm SEM. Twelve SCN explants were used.

(G) Rescue of circadian behavioral phenotypes in *Eif4ebp1* KO mice by PG99-465. Representative double-plotted actograms of wheel-running activities of a vehicle-infused (left) and a PG99-465-infused mouse (right). The *Eif4ebp1* KO mice were cannulated and entrained to a 12 hr/12 hr light/dark (LD) cycle for 10 days, and on the 11th day, mice were infused with 4 μ l saline or PG99-465 (100 μ M) at ZT15, and the light cycle was advanced for 6 hr (light on at ZT18). Red asterisks indicate the time of infusion and red arrows (right) indicate the day when the light cycle was shifted.

(H) Line graphs showing the daily phase advance of wheel-running activities of the *Eif4ebp1* KO mice following a 6 hr advancing light cycle shift. Values are presented as the mean \pm SEM. Each data point is averaged from six mice. * $p < 0.05$ PG99-465 versus vehicle by ANOVA.

Decreased VIP and Increased Susceptibility to LL-Induced Clock Desynchrony in *Mtor*^{+/-} mice

mTOR phosphorylates 4E-BP1 and decreases its translational inhibitory activity in the SCN (Cao et al., 2008). To corroborate the regulation of VIP and the clock function by 4E-BP1, we utilized an *Mtor*^{+/-} mouse strain. In the *Mtor*^{+/-} SCN, VIP was decreased by ~50% (*Mtor*^{+/-} versus *Mtor*^{+/+}, $p < 0.05$, Student's t test; Figure 7A). In the *Mtor*^{+/-} brain, mTOR activity was decreased, as indicated by decreased phosphorylation of 4E-BP1 (normalized

band intensities: *Mtor*^{+/-} versus *Mtor*^{+/+}, at Thr70: 0.69 ± 0.04 versus 1 ± 0.07 ; at Ser65: 0.67 ± 0.07 versus 1 ± 0.19 , $p < 0.05$, Student's t test), and prepro-VIP was reduced (normalized band intensities: *Mtor*^{+/-} versus *Mtor*^{+/+}, 0.43 ± 0.08 versus 1 ± 0.08 , $p < 0.05$, Student's t test; Figure 7B).

To investigate the effects of lower VIP level on the circadian clock function, we monitored circadian behavior of the *Mtor*^{+/-} mice in LL. Mice were housed in regular cages in LL (200 lx) for 14 days and then transferred to cages equipped with running

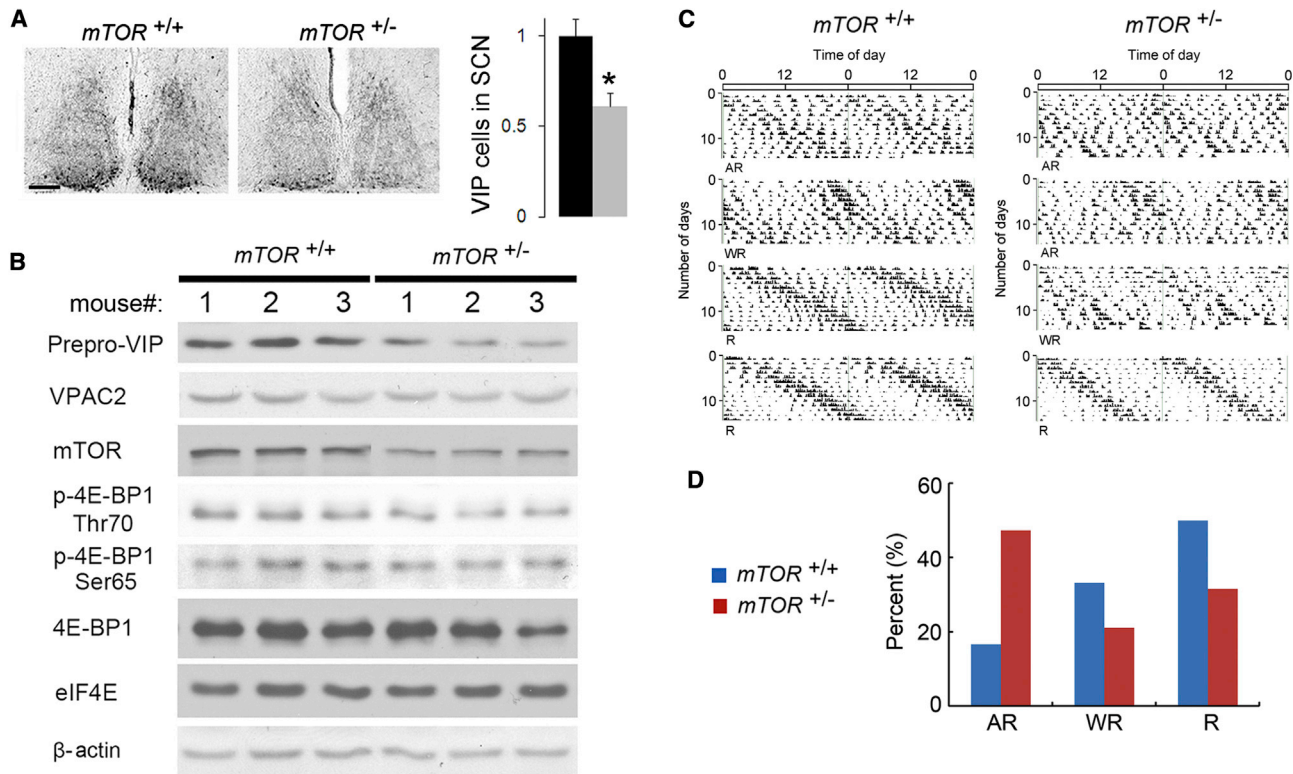


Figure 7. Decreased VIP Expression and Increased Susceptibility to Constant Light-Induced Clock Desynchrony in *Mtor*^{+/-} Mice

(A) Representative bright-field microscopy images showing VIP immunostaining in the SCN. Mice were entrained and sacrificed at ZT0. Quantitation of VIP expression in the SCN is shown to the right. The values are presented as the mean ± SEM. Five mice were used for each group. **p* < 0.05 by Student's *t* test. Note that number of VIP-positive cells was decreased in the *Mtor*^{+/-} SCN. Scale bars: 100 μm.

(B) Western blots of whole-forebrain lysates. Animals were sacrificed at ZT0. The numbers 1–3 indicate three different animals for each group. Note that mTOR expression and 4E-BP1 phosphorylation were decreased in the brains of *Mtor*^{+/-} animals. Accordingly, prepro-VIP but not VPAC2 expression was decreased in these mice. eIF4E and β-actin were used as loading controls. See Results for quantitation of the blots.

(C and D) Representative wheel-running actograms of mice in constant light (C). Actograms from four *Mtor*^{+/+} (left) and four *Mtor*^{+/-} (right) mice are shown. R, rhythmic; AR, arrhythmic; WR, weakly rhythmic. Note that more *Mtor*^{+/-} mice exhibited arrhythmic behavior compared to *Mtor*^{+/+} mice. The percentages of three types of behavior are shown in (D).

wheels in LL (55 lx) to record their circadian behavior for 14 days. LL induced three types of behavior (R, AR, and WR) in both *Mtor*^{+/-} and *Mtor*^{+/+} animals. A larger percentage of *Mtor*^{+/-} mice (47.4%, 9/19) exhibited arrhythmic behavior than did *Mtor*^{+/+} mice (16.7%, 3/18) (*p* < 0.05, χ^2 test; Figures 7C and 7D), indicating increased susceptibility to LL-induced clock desynchrony in *Mtor*^{+/-} mice. Taken together, the results demonstrate that mTOR/4E-BP1 signaling bidirectionally regulates VIP level and susceptibility of the SCN clock to desynchronizing effect of LL.

DISCUSSION

In the present study, we found that mTOR signaling promotes *Vip* mRNA translation by repressing 4E-BP1. Consequently, in *Eif4ebp1* KO mice, VIP is increased in the SCN, which is associated with a larger amplitude of PER2 rhythms, accelerated circadian clock entrainment, and enhanced synchrony. The phenotypes can be reversed by pharmacologically antagonizing VIP signaling and in *Mtor*^{+/-} mice, in which VIP is decreased in

the SCN. The findings demonstrate a key role for mTOR/4E-BP1-mediated translational control in the SCN circadian clock physiology.

Our findings indicate that entrainment and synchrony of the SCN clock are enhanced in *Eif4ebp1* KO mice. This conclusion is based on three lines of evidence: First, *Eif4ebp1* KO mice re-entrain faster to a shifted LD cycle than WT littermates. Photic entrainment of the SCN clock involves photic reception and resynchronization within the SCN cells. The photic input pathway appears to be normal in the KO mice. However, cellular PER rhythms resynchronize faster in their SCN. Importantly, the temporal profile of PER rhythm resynchronization is consistent with the progress of animal behavioral re-entrainment, suggesting that faster resynchronization of molecular rhythms in the SCN underlies accelerated behavioral re-entrainment. Second, *Eif4ebp1* KO mice are more resistant to forced clock desynchrony by constant light. Constant light disrupts intercellular synchrony but does not affect individual cellular clocks in the SCN (Ohta et al., 2005). More resistance to constant light is consistent with enhanced synchrony among SCN cells in

*Eif4ebp1*KO mice. Conversely, in *Mtor*^{+/-} mice in which 4E-BP1 activity is enhanced, the SCN clock is more susceptible to the disruptive effects of constant light, consistent with compromised synchrony in the SCN of *Mtor*^{+/-} mice. Third, SCN explants of *Eif4ebp1*KO mice display higher amplitudes of PER2::LUC rhythms. As there is no change in amplitude and period in peripheral oscillators, a plausible explanation is that coupling strength among SCN cells is increased in the *Eif4ebp1*KO mice, and consequently the amplitude of circadian rhythms is increased at the tissue level.

Mounting evidence has established VIP as an essential mediator of SCN synchrony (Shen et al., 2000; Harmar et al., 2002; Colwell et al., 2003; Aton et al., 2005; Maywood et al., 2006). For example, microinjection of VIP induces phase shifts in the SCN circadian pacemaker, and VIP antagonists disrupt circadian function (Piggins et al., 1995; Gozes et al., 1995; Reed et al., 2001; Cutler, et al., 2003). VIP- (Colwell et al., 2003) and VPAC2-deficient mice (Harmar et al., 2002) show arrhythmic wheel-running behavior in constant darkness. Electrophysiological recordings show that SCN neurons in slices from *Vip*^{-/-} and *Vipr2*^{-/-} (encoding VPAC2) mice do not exhibit circadian rhythms of firing and lack interneuronal synchrony. Daily application of a VIP agonist to the *Vip*^{-/-} SCN restores synchrony (Aton et al., 2005). Similarly, bioluminescence recordings from *Vipr2*^{-/-} SCN slices also suggest that VIP signaling is necessary to synchronize individual SCN neurons as well as to maintain intracellular rhythms within these cells (Maywood et al., 2006, 2011).

4E-BP1 represses prepro-VIP synthesis by inhibiting *Vip* mRNA translation. In *Eif4ebp1* KO mice, VIP expression is constitutively upregulated in the SCN due to overexpression of prepro-VIP. Compared with transcriptional control, translational regulation of *Vip* by 4E-BP1 does not significantly affect the phase of VIP daily rhythms (Takahashi et al., 1989); rather, it increases the abundance of VIP throughout the 24 hr cycle. Of note, upregulating VIP signaling is sufficient to accelerate entrainment of the SCN circadian clock. For example, in *Vipr2* transgenic mice, where VPAC2 is constitutively overexpressed, re-entrainment of circadian behavioral rhythms to a shifted LD cycle is accelerated and animals exhibit a shorter circadian behavioral period (Shen et al., 2000). Moreover, pharmacological application of VIP facilitates behavioral re-entrainment to a shifted LD cycle and re-entrainment of PER rhythms in SCN slices to a changed temperature cycle (An, 2011a). To further link the phenotype of the *Eif4ebp1* KO mice to VIP signaling, we applied the VPAC2 antagonist PG99-465 to the SCN and demonstrate that VIP antagonism can reverse the faster-entrainment phenotype of *Eif4ebp1* KO mice and decrease the amplitude of PER2::LUC rhythms in the KO SCN explants.

In the SCN, VIP is rhythmically released by a subset of neurons in the core region that receives direct synaptic inputs from the retina (Welsh et al., 2010). Its receptor, VPAC2, is expressed in about 60% of SCN neurons, including half of the VIPergic neurons and almost all AVP-expressing neurons in the shell region (Abrahamson and Moore, 2001; An et al., 2012). VIP depolarizes SCN neurons by closing potassium channels and induces *Per1* and *Per2* expression via parallel changes in adenylate cyclase and phospholipase C activities (Nielsen et al., 2002; Meyer-

Spasche and Piggins 2004; An et al., 2011b). Synaptic inputs from the core SCN synchronize neurons in the shell region, consistent with dense anatomical projections from the core to the shell but sparse reciprocal projections (Abrahamson and Moore, 2001). Resetting to a shifted LD cycle is initiated by phase shifts of a small group of core SCN neurons that are quickly synchronized (indicated by clock gene expression and firing rates) following the LD cycle shift (Nagano et al., 2003; Rohling et al., 2011). In turn, these neurons synchronize those in the shell region via GABAergic and neuropeptidergic synaptic transmission (Albus et al., 2005; Maywood et al., 2006, 2011).

Although VIPergic synaptic transmission is known to be essential for SCN synchrony in general, its role in core-shell synchronization during the SCN entrainment is not fully appreciated. The degree of core-shell synchronization contributes to the ability of the SCN pacemaker to reset (Rohling et al., 2011). Conceivably, increased VIP levels would enhance the efficacy of synaptic transmission from the core to the shell region and thereby accelerate synchronization of the shell by the core. This model is supported by the close correlation between increased VIP expression, faster clock protein resynchronization, and accelerated behavioral entrainment in the *Eif4ebp1* KO mice. Under conditions of “forced clock desynchrony” such as a 22 hr LD cycle or constant light, the rhythms from the core and the shell can become out of phase and animals show split behavioral rhythms or become arrhythmic (de la Iglesia et al., 2004; Ohta et al., 2005). Similar to the role in entrainment, enhanced VIPergic synaptic transmission from the core to the shell would make the SCN ensemble more strongly coupled and thus more resistant to the desynchronizing effects of these conditions, whereas decreased VIP level would make the clock more susceptible to the clock-disruptive effects. This model is consistent with the opposite changes of susceptibility to constant light in *Eif4ebp1* KO and *Mtor*^{+/-} mice.

In addition to VIP, we examined other mediators of SCN synchrony such as GRP and GABA that may underlie the phenotypes of 4E-BP1 mutants. The expression of the relevant proteins is not altered in the 4E-BP1 KO mice, thus not supporting a role for these mediators in regulation of the clock by 4E-BP1. A previous study showed that mTOR signaling modulates photic entrainment of the SCN clock by facilitating PER1 and PER2 expression (Cao et al., 2010). Although 4E-BP1 is a downstream effector of mTOR, pharmacological disruption (i.e., using rapamycin) of mTOR signaling in vivo only transiently inhibits 4E-BP1 activity (up to a couple of hours, unpublished data) and thus cannot be used to study circadian functions of 4E-BP1. Here we show that 4E-BP1 does not regulate PER1 and PER2 expression. Thus, the effects of mTOR on PER expression are mediated through other mTOR downstream targets.

Besides its role in *Vip* regulation, 4E-BP1 may have other functions in circadian clocks. 4E-BP1 inhibits translational initiation by binding to eIF4E and impairing the formation of the translational preinitiation complex, which consists of eIF4E, eIF4A, and eIF4G. Indeed, several studies have reported the roles of the eIF4E and its binding proteins in circadian clock physiology. For example, knockdown of the eIF4G homolog, NAT1, significantly reduces PER expression and lengthens the behavioral period in *Drosophila* (Bradley et al., 2012). Moreover, a recent

study reported that the clock coordinates ribosomal biogenesis in the liver by rhythmic activation of the mTOR/4E-BP1/eIF4E pathway (Jouffe et al., 2013). Therefore, circadian rhythmicity of the mTOR/4E-BP1 signaling may be a general feature of circadian oscillators. Regulation of *Vip* mRNA translation is a SCN (or VIP-producing tissue)-specific function of the mTOR/4E-BP1 signaling. In the peripheral oscillators, where there is no obvious role for VIP or circadian coupling, the mTOR/4E-BP1 pathway may serve as an output signaling of the circadian clock to coordinate rhythmic mRNA translation.

EXPERIMENTAL PROCEDURES

Animals

Eif4ebp1 KO mice (Tsukiyama-Kohara et al., 2001) were backcrossed to WT C57BL/6 mice for over ten generations to obtain a pure C57BL/6 background. *mtor* floxed mice on a C57BL/6 background (kindly provided by Dr. Sara C. Kozma, University of Cincinnati) were crossed to cytomegalovirus promoter (a ubiquitously expressed promoter)-Cre mice to generate *mtor*^{-/-} mice (Sauer and Henderson, 1988). *Eif4ebp1* KO mice were crossed with mPER2::LUC transgenic reporter mice (Yoo et al., 2004) to obtain *Eif4ebp1*^{-/-}:mPER2::LUC mice. Animals were maintained in the animal facility at McGill University in accordance with institutional guidelines. All procedures were approved by the Institutional Animal Care and Use Committee.

Cannulation and Infusion

Mice were cannulated in the lateral ventricles using the techniques described by Cao et al. (2008). The coordinates (posterior, 0.34 mm from bregma; lateral, 0.90 mm from the midline; dorsoventral, -2.15 mm from bregma) were used to place the tip of a 24 gauge guide cannula into the lateral ventricle. To disrupt VIP signaling, PG99-465 (100 μ M, 4 μ l; Bachem, Switzerland) was infused through the cannula at ZT15. Control animals were infused with physiological saline (4 μ l).

Circadian Behavioral Assay

Eight- to 10-week-old male mice were individually housed in cages equipped with running wheels. Wheel rotation was recorded using the VitalView program (Mini Mitter, Bend, OR, USA) (Hood et al., 2010). For the "jet lag" experiments, mice were entrained to a 12 hr/12 hr LD cycle (12 lx) for 10 days. On the 11th day, the LD cycle was either advanced for 6 hr or delayed for 10 hr, and animal behavior was recorded for 10 days following the LD cycle shift. For the constant light (LL) experiments, mice were first kept in common cages under LL (200 lx) for 14 days and then transferred to running-wheel cages in LL (55 lx) to record their intrinsic rhythms for 14 days. The actograms of wheel-running activities were analyzed using the ActiView software (Mini Mitter) and the ClockLab software (Actimetrics, Wilmette, OR, USA).

Brain Tissue Processing, Immunostaining, and Microscopic Imaging Analysis

Under indicated conditions, mice were sacrificed and brain tissue was harvested. SCN sections were processed and immunostained for 4E-BP1, p-4E-BP1, PER1, PER2, AVP, and VIP as previously reported (Cao et al., 2008, 2010, 2011). Bright-field microscopy images were captured using a digital camera mounted on an inverted Zeiss microscope (Oberkochen, Germany). Confocal microscopy images were captured using a Zeiss 510 Meta confocal microscope. See Supplemental Information for antibody information and image quantitation methods.

Protein Extraction and Western Blotting Analysis

The SCN tissue was excised using a 700 μ m tissue punch and frozen on dry ice. SCN tissue was pooled from five animals per condition. Brain tissue was homogenized with a pestal grinder (Fisher Scientific Limited, Nepean, Canada) and lysed using a lysis buffer previously reported (Lee, 2007). Western blotting analysis was performed as described (Dowling et al., 2010).

Brain Polysome Profiling

Brain polysome profiling was performed as described (Gkogkas et al., 2013). The polysome to monosome ratio was calculated as the area under the A_{254} absorbance curve, using the absorbance values processed with the definite integral command in MATLAB.

Real-Time Quantitative Reverse Transcription-PCR

RNA extraction and qRT-PCR were performed as reported (Dowling et al., 2010). See Supplemental Information for primer information.

Explant Culture, Kinetic Bioluminescence Recording, and Data Analysis

Explants of SCN and lung tissues from *Eif4ebp1*^{-/-}:mPER2::LUC and mPER2::LUC mice were dissected and cultured as reported (Liu et al., 2007b). Real-time circadian reporter assays were performed using a LumiCycle luminometer (Actimetrics, Inc.) as previously described (Khan et al., 2012). Baseline-subtracted data (counts/second) were plotted against time (days) in culture. For comparison, the first peak was aligned in the plotted data. The LumiCycle Analysis program (version 2.31, Actimetrics, Inc.) was used to analyze rhythm parameters. For period length analysis, raw data were baseline fitted, and the baseline-subtracted data were fitted to a sine wave (damped), from which the period was determined. All samples showed persistent rhythms and goodness-of-fit of > 90% was achieved. For amplitude analysis, baseline-subtracted data (polynomial order = 1; days 3–6 of recording data) were fitted to a sine wave, from which the amplitude was determined using Sin Fit.

Statistical Analysis

The values are presented as the mean \pm standard error of the mean (SEM) or percentage (%). Statistical analysis was performed using SPSS software (SPSS Inc, Chicago, IL, USA). Mean values from multiple groups were compared via one-way ANOVA, followed by the Student-Newman-Keuls test. Mean values from two groups were compared via Student's *t* test. Arrhythmia rates of WT and KO mice were compared via the χ^2 test. *p* < 0.05 was considered as statistically significant.

SUPPLEMENTAL INFORMATION

Supplemental Information includes four figures, two tables, and Supplemental Experimental Procedures and can be found with this article online at <http://dx.doi.org/10.1016/j.neuron.2013.06.026>.

ACKNOWLEDGMENTS

We thank Michael Rosbash, Isaac Edery, Erik Herzog, and Jane Stewart for advice and critical reading of the manuscript and Maritza Jaramillo, Alex Gavrila, Annie Sylvestre, and Isabelle Harvey for excellent technical assistance. We are indebted to Joseph Takahashi for his generous gift of the mPER2::LUC transgenic mice, Sara C. Kozma for the *mtor* floxed mice, and Linda Penn and Manfred Schwab for the SHEP neuroblastoma cell line. This work was supported by Canadian Institute of Health Research (CIHR) Grants MOP 114994 to N.S. and MOP 13625 to S.A. and by National Science Foundation (NSF) Grant IOS-0920417 to A.C.L.. N.S. is a senior international research scholar of the Howard Hughes Medical Institute (HHMI). R.C. is a Fonds de recherche du Québec – Santé (FRQS) Postdoctoral Training Award recipient.

Accepted: June 17, 2013

Published: August 21, 2013

REFERENCES

- Abraham, U., Granada, A.E., Westermark, P.O., Heine, M., Kramer, A., and Herzog, H. (2010). Coupling governs entrainment range of circadian clocks. *Mol. Syst. Biol.* 6, 438.
- Abrahamson, E.E., and Moore, R.Y. (2001). Suprachiasmatic nucleus in the mouse: retinal innervation, intrinsic organization and efferent projections. *Brain Res.* 916, 172–191.

- Albus, H., Vansteensel, M.J., Michel, S., Block, G.D., and Meijer, J.H. (2005). A GABAergic mechanism is necessary for coupling dissociable ventral and dorsal regional oscillators within the circadian clock. *Curr. Biol.* *15*, 886–893.
- Amir, S., Lamont, E.W., Robinson, B., and Stewart, J. (2004). A circadian rhythm in the expression of PERIOD2 protein reveals a novel SCN-controlled oscillator in the oval nucleus of the bed nucleus of the stria terminalis. *J. Neurosci.* *24*, 781–790.
- An, S. (2011a). The Roles of Vasoactive Intestinal Polypeptide in Circadian Entrainment of Suprachiasmatic Nucleus. Doctoral dissertation, Washington University in St. Louis: ProQuest/UMI. (pqid:2342376571.)
- An, S., Irwin, R.P., Allen, C.N., Tsai, C., and Herzog, E.D. (2011b). Vasoactive intestinal polypeptide requires parallel changes in adenylate cyclase and phospholipase C to entrain circadian rhythms to a predictable phase. *J. Neurophysiol.* *105*, 2289–2296.
- An, S., Tsai, C., Ronecker, J., Bayly, A., and Herzog, E.D. (2012). Spatiotemporal distribution of vasoactive intestinal polypeptide receptor 2 in mouse suprachiasmatic nucleus. *J. Comp. Neurol.* *520*, 2730–2741.
- Antle, M.C., and Silver, R. (2005). Orchestrating time: arrangements of the brain circadian clock. *Trends Neurosci.* *28*, 145–151.
- Aton, S.J., and Herzog, E.D. (2005). Come together, right...now: synchronization of rhythms in a mammalian circadian clock. *Neuron* *48*, 531–534.
- Aton, S.J., Colwell, C.S., Harmar, A.J., Waschek, J., and Herzog, E.D. (2005). Vasoactive intestinal polypeptide mediates circadian rhythmicity and synchrony in mammalian clock neurons. *Nat. Neurosci.* *8*, 476–483.
- Bradley, S., Narayanan, S., and Rosbash, M. (2012). NAT1/DAP5/p97 and atypical translational control in the *Drosophila* Circadian Oscillator. *Genetics* *192*, 943–957.
- Cao, R., and Obrietan, K. (2010). mTOR Signaling and Entrainment of the Mammalian Circadian Clock. *Mol Cell Pharmacol* *2*, 125–130.
- Cao, R., Lee, B., Cho, H.Y., Saklayen, S., and Obrietan, K. (2008). Photic regulation of the mTOR signaling pathway in the suprachiasmatic circadian clock. *Mol. Cell. Neurosci.* *38*, 312–324.
- Cao, R., Li, A., and Cho, H.Y. (2009). mTOR signaling in epileptogenesis: too much of a good thing? *J. Neurosci.* *29*, 12372–12373.
- Cao, R., Li, A., Cho, H.Y., Lee, B., and Obrietan, K. (2010). Mammalian target of rapamycin signaling modulates photic entrainment of the suprachiasmatic circadian clock. *J. Neurosci.* *30*, 6302–6314.
- Cao, R., Anderson, F.E., Jung, Y.J., Dziema, H., and Obrietan, K. (2011). Circadian regulation of mammalian target of rapamycin signaling in the mouse suprachiasmatic nucleus. *Neuroscience* *181*, 79–88.
- Colwell, C.S., Michel, S., Itri, J., Rodriguez, W., Tam, J., Lelievre, V., Hu, Z., Liu, X., and Waschek, J.A. (2003). Disrupted circadian rhythms in VIP- and PH1-deficient mice. *Am. J. Physiol. Regul. Integr. Comp. Physiol.* *285*, R939–R949.
- Costa-Mattioli, M., Sossin, W.S., Klann, E., and Sonenberg, N. (2009). Translational control of long-lasting synaptic plasticity and memory. *Neuron* *61*, 10–26.
- Cota, D., Proulx, K., Smith, K.A., Kozma, S.C., Thomas, G., Woods, S.C., and Seeley, R.J. (2006). Hypothalamic mTOR signaling regulates food intake. *Science* *312*, 927–930.
- Cutler, D.J., Haraura, M., Reed, H.E., Shen, S., Sheward, W.J., Morrison, C.F., Marston, H.M., Harmar, A.J., and Piggins, H.D. (2003). The mouse VPAC2 receptor confers suprachiasmatic nuclei cellular rhythmicity and responsiveness to vasoactive intestinal polypeptide in vitro. *Eur. J. Neurosci.* *17*, 197–204.
- Daan, S., and Pittendrigh, C.S. (1976). A Functional Analysis of Circadian Pacemakers in Nocturnal Rodents III. Heavy Water and Constant Light: Homeostasis of Frequency? *J. Comp. Physiol.* *106*, 253–266.
- Davidson, A.J., Castanon-Cervantes, O., Leise, T.L., Molyneux, P.C., and Harrington, M.E. (2009). Visualizing jet lag in the mouse suprachiasmatic nucleus and peripheral circadian timing system. *Eur. J. Neurosci.* *29*, 171–180.
- de la Iglesia, H.O., Cambras, T., Schwartz, W.J., and Díez-Noguera, A. (2004). Forced desynchronization of dual circadian oscillators within the rat suprachiasmatic nucleus. *Curr. Biol.* *14*, 796–800.
- Dowling, R.J., Topisirovic, I., Alain, T., Bidinosti, M., Fonseca, B.D., Petroulakis, E., Wang, X., Larsson, O., Selvaraj, A., Liu, Y., et al. (2010). mTORC1-mediated cell proliferation, but not cell growth, controlled by the 4E-BPs. *Science* *328*, 1172–1176.
- Field, M.D., Maywood, E.S., O'Brien, J.A., Weaver, D.R., Reppert, S.M., and Hastings, M.H. (2000). Analysis of clock proteins in mouse SCN demonstrates phylogenetic divergence of the circadian clockwork and resetting mechanisms. *Neuron* *25*, 437–447.
- Gingras, A.C., Gygi, S.P., Raught, B., Polakiewicz, R.D., Abraham, R.T., Hoekstra, M.F., Aebersold, R., and Sonenberg, N. (1999). Regulation of 4E-BP1 phosphorylation: a novel two-step mechanism. *Genes Dev.* *13*, 1422–1437.
- Gkogkas, C.G., Khoutorsky, A., Ran, I., Rampakakis, E., Nevarko, T., Weatherill, D.B., Vasuta, C., Yee, S., Truitt, M., Dallaire, P., et al. (2013). Autism-related deficits via dysregulated eIF4E-dependent translational control. *Nature* *493*, 371–377.
- Gozes, I., and Brenneman, D.E. (1989). VIP: molecular biology and neurobiological function. *Mol. Neurobiol.* *3*, 201–236.
- Gozes, I., Lilling, G., Glazer, R., Ticher, A., Ashkenazi, I.E., Davidson, A., Rubinraut, S., Fridkin, M., and Brenneman, D.E. (1995). Superactive lipophilic peptides discriminate multiple vasoactive intestinal peptide receptors. *J. Pharmacol. Exp. Ther.* *273*, 161–167.
- Harmar, A.J., Marston, H.M., Shen, S., Spratt, C., West, K.M., Sheward, W.J., Morrison, C.F., Dorin, J.R., Piggins, H.D., Reubi, J.C., et al. (2002). The VPAC(2) receptor is essential for circadian function in the mouse suprachiasmatic nuclei. *Cell* *109*, 497–508.
- Hastings, M.H., Field, M.D., Maywood, E.S., Weaver, D.R., and Reppert, S.M. (1999). Differential regulation of mPER1 and mTIM proteins in the mouse suprachiasmatic nuclei: new insights into a core clock mechanism. *J. Neurosci.* *19*, RC11.
- Herzog, E.D., Takahashi, J.S., and Block, G.D. (1998). Clock controls circadian period in isolated suprachiasmatic nucleus neurons. *Nat. Neurosci.* *1*, 708–713.
- Hood, S., Cassidy, P., Cossette, M.P., Weigl, Y., Verwey, M., Robinson, B., Stewart, J., and Amir, S. (2010). Endogenous dopamine regulates the rhythm of expression of the clock protein PER2 in the rat dorsal striatum via daily activation of D2 dopamine receptors. *J. Neurosci.* *30*, 14046–14058.
- Jouffe, C., Cretenet, G., Symul, L., Martin, E., Atger, F., Naef, F., and Gachon, F. (2013). The circadian clock coordinates ribosome biogenesis. *PLoS Biol.* *11*, e1001455.
- Khan, S.K., Xu, H., Ukai-Tadenuma, M., Burton, B., Wang, Y., Ueda, H.R., and Liu, A.C. (2012). Identification of a novel cryptochrome differentiating domain required for feedback repression in circadian clock function. *J. Biol. Chem.* *287*, 25917–25926.
- Kornhauser, J.M., Nelson, D.E., Mayo, K.E., and Takahashi, J.S. (1992). Regulation of jun-B messenger RNA and AP-1 activity by light and a circadian clock. *Science* *255*, 1581–1584.
- Laplanche, M., and Sabatini, D.M. (2012). mTOR signaling in growth control and disease. *Cell* *149*, 274–293.
- Lee, C. (2007). Protein extraction from mammalian tissues. *Methods Mol. Biol.* *362*, 385–389.
- Liu, C., and Reppert, S.M. (2000). GABA synchronizes clock cells within the suprachiasmatic circadian clock. *Neuron* *25*, 123–128.
- Liu, A.C., Lewis, W.G., and Kay, S.A. (2007a). Mammalian circadian signaling networks and therapeutic targets. *Nat. Chem. Biol.* *3*, 630–639.
- Liu, A.C., Welsh, D.K., Ko, C.H., Tran, H.G., Zhang, E.E., Priest, A.A., Buhr, E.D., Singer, O., Meeker, K., Verma, I.M., et al. (2007b). Intercellular coupling confers robustness against mutations in the SCN circadian clock network. *Cell* *129*, 605–616.

- Long, M.A., Jutras, M.J., Connors, B.W., and Burwell, R.D. (2005). Electrical synapses coordinate activity in the suprachiasmatic nucleus. *Nat. Neurosci.* **8**, 61–66.
- Maywood, E.S., Reddy, A.B., Wong, G.K., O'Neill, J.S., O'Brien, J.A., McMahon, D.G., Hattar, A.J., Okamura, H., and Hastings, M.H. (2006). Synchronization and maintenance of timekeeping in suprachiasmatic circadian clock cells by neuropeptidergic signaling. *Curr. Biol.* **16**, 599–605.
- Maywood, E.S., Chesham, J.E., O'Brien, J.A., and Hastings, M.H. (2011). A diversity of paracrine signals sustains molecular circadian cycling in suprachiasmatic nucleus circuits. *Proc. Natl. Acad. Sci. USA* **108**, 14306–14311.
- Meyer-Spasche, A., and Piggins, H.D. (2004). Vasoactive intestinal polypeptide phase-advances the rat suprachiasmatic nuclei circadian pacemaker in vitro via protein kinase A and mitogen-activated protein kinase. *Neurosci. Lett.* **358**, 91–94.
- Nagano, M., Adachi, A., Nakahama, K., Nakamura, T., Tamada, M., Meyer-Bernstein, E., Sehgal, A., and Shigeyoshi, Y. (2003). An abrupt shift in the day/night cycle causes desynchrony in the mammalian circadian center. *J. Neurosci.* **23**, 6141–6151.
- Nakamura, W., Yamazaki, S., Takasu, N.N., Mishima, K., and Block, G.D. (2005). Differential response of Period 1 expression within the suprachiasmatic nucleus. *J. Neurosci.* **25**, 5481–5487.
- Nielsen, H.S., Hannibal, J., and Fahrenkrug, J. (2002). Vasoactive intestinal polypeptide induces per1 and per2 gene expression in the rat suprachiasmatic nucleus late at night. *Eur. J. Neurosci.* **15**, 570–574.
- Obrietan, K., Impey, S., and Storm, D.R. (1998). Light and circadian rhythmicity regulate MAP kinase activation in the suprachiasmatic nuclei. *Nat. Neurosci.* **1**, 693–700.
- Ohta, H., Yamazaki, S., and McMahon, D.G. (2005). Constant light desynchronizes mammalian clock neurons. *Nat. Neurosci.* **8**, 267–269.
- Piggins, H.D., Antle, M.C., and Rusak, B. (1995). Neuropeptides phase shift the mammalian circadian pacemaker. *J. Neurosci.* **15**, 5612–5622.
- Reddy, A.B., Field, M.D., Maywood, E.S., and Hastings, M.H. (2002). Differential resynchronization of circadian clock gene expression within the suprachiasmatic nuclei of mice subjected to experimental jet lag. *J. Neurosci.* **22**, 7326–7330.
- Reed, H.E., Meyer-Spasche, A., Cutler, D.J., Coen, C.W., and Piggins, H.D. (2001). Vasoactive intestinal polypeptide (VIP) phase-shifts the rat suprachiasmatic nucleus clock in vitro. *Eur. J. Neurosci.* **13**, 839–843.
- Reppert, S.M., and Weaver, D.R. (2002). Coordination of circadian timing in mammals. *Nature* **418**, 935–941.
- Rohling, J.H., vanderLeest, H.T., Michel, S., Vansteensel, M.J., and Meijer, J.H. (2011). Phase resetting of the mammalian circadian clock relies on a rapid shift of a small population of pacemaker neurons. *PLoS ONE* **6**, e25437.
- Rosbash, M. (2009). The implications of multiple circadian clock origins. *PLoS Biol.* **7**, e62.
- Rosbash, M., Bradley, S., Kadener, S., Li, Y., Luo, W., Menet, J.S., Nagoshi, E., Palm, K., Schoer, R., Shang, Y., and Tang, C.H. (2007). Transcriptional feedback and definition of the circadian pacemaker in *Drosophila* and animals. *Cold Spring Harb. Symp. Quant. Biol.* **72**, 75–83.
- Sauer, B., and Henderson, N. (1988). Site-specific DNA recombination in mammalian cells by the Cre recombinase of bacteriophage P1. *Proc. Natl. Acad. Sci. USA* **85**, 5166–5170.
- Shen, S., Spratt, C., Sheward, W.J., Kalló, I., West, K., Morrison, C.F., Coen, C.W., Marston, H.M., and Hattar, A.J. (2000). Overexpression of the human VPAC2 receptor in the suprachiasmatic nucleus alters the circadian phenotype of mice. *Proc. Natl. Acad. Sci. USA* **97**, 11575–11580.
- Sonenberg, N., and Hinnebusch, A.G. (2009). Regulation of translation initiation in eukaryotes: mechanisms and biological targets. *Cell* **136**, 731–745.
- Takahashi, Y., Okamura, H., Yanaihara, N., Hamada, S., Fujita, S., and Ibata, Y. (1989). Vasoactive intestinal peptide immunoreactive neurons in the rat suprachiasmatic nucleus demonstrate diurnal variation. *Brain Res.* **497**, 374–377.
- Takahashi, J.S., Hong, H.K., Ko, C.H., and McDearmon, E.L. (2008). The genetics of mammalian circadian order and disorder: implications for physiology and disease. *Nat. Rev. Genet.* **9**, 764–775.
- To, T.L., Henson, M.A., Herzog, E.D., and Doyle, F.J., 3rd. (2007). A molecular model for intercellular synchronization in the mammalian circadian clock. *Biophys. J.* **92**, 3792–3803.
- Topisirovic, I., and Sonenberg, N. (2011). mRNA translation and energy metabolism in cancer: the role of the MAPK and mTORC1 pathways. *Cold Spring Harb. Symp. Quant. Biol.* **76**, 355–367.
- Tsukiyama-Kohara, K., Poulin, F., Kohara, M., DeMaria, C.T., Cheng, A., Wu, Z., Gingras, A.C., Katsume, A., Elchebly, M., Spiegelman, B.M., et al. (2001). Adipose tissue reduction in mice lacking the translational inhibitor 4E-BP1. *Nat. Med.* **7**, 1128–1132.
- vanderLeest, H.T., Rohling, J.H., Michel, S., and Meijer, J.H. (2009). Phase shifting capacity of the circadian pacemaker determined by the SCN neuronal network organization. *PLoS ONE* **4**, e4976.
- Waschek, J.A., Hsu, C.M., and Eiden, L.E. (1988). Lineage-specific regulation of the vasoactive intestinal peptide gene in neuroblastoma cells is conferred by 5.2 kilobases of 5'-flanking sequence. *Proc. Natl. Acad. Sci. USA* **85**, 9547–9551.
- Welsh, D.K., Logothetis, D.E., Meister, M., and Reppert, S.M. (1995). Individual neurons dissociated from rat suprachiasmatic nucleus express independently phased circadian firing rhythms. *Neuron* **14**, 697–706.
- Welsh, D.K., Takahashi, J.S., and Kay, S.A. (2010). Suprachiasmatic nucleus: cell autonomy and network properties. *Annu. Rev. Physiol.* **72**, 551–577.
- Yamaguchi, S., Isejima, H., Matsuo, T., Okura, R., Yagita, K., Kobayashi, M., and Okamura, H. (2003). Synchronization of cellular clocks in the suprachiasmatic nucleus. *Science* **302**, 1408–1412.
- Yamazaki, S., Numano, R., Abe, M., Hida, A., Takahashi, R., Ueda, M., Block, G.D., Sakaki, Y., Menaker, M., and Tei, H. (2000). Resetting central and peripheral circadian oscillators in transgenic rats. *Science* **288**, 682–685.
- Yoo, S.H., Yamazaki, S., Lowrey, P.L., Shimomura, K., Ko, C.H., Buhr, E.D., Slepka, S.M., Hong, H.K., Oh, W.J., Yoo, O.J., et al. (2004). PERIOD2:LUCIFERASE real-time reporting of circadian dynamics reveals persistent circadian oscillations in mouse peripheral tissues. *Proc. Natl. Acad. Sci. USA* **101**, 5339–5346.
- Zheng, X., and Sehgal, A. (2010). AKT and TOR signaling set the pace of the circadian pacemaker. *Curr. Biol.* **20**, 1203–1208.